

Bicellar Mixtures Containing Pluronic F68: Morphology and Lateral Diffusion from Combined SANS and PFG NMR Studies

Ronald Soong,[†] Mu-Ping Nieh,[‡] Eric Nicholson,[§] John Katsaras,[‡] and Peter M. Macdonald^{*†}

[†]Department of Chemical and Physical Sciences, University of Toronto Mississauga, 3359 Mississauga Road North, Mississauga, Ontario, Canada L5L 1C6, [‡]National Research Council of Canada, Chalk River Laboratories, Chalk River, Ontario, Canada K0J 1J0, and [§]Division of Engineering Science, University of Toronto, 40 St. George Street, Toronto, Ontario, Canada M5S 2E4

Received July 29, 2009. Revised Manuscript Received September 9, 2009

Small angle neutron scattering (SANS) and pulsed field gradient (PFG) nuclear magnetic resonance (NMR) diffusion measurements were applied to examine morphology and diffusion in dimyristoyl- plus dihexanoyl-phosphatidylcholine bicellar mixtures, either neutral or negatively charged, incorporating a Pluronic triblock copolymer (F68). Negatively charged bicellar mixtures, doped with dimyristoylphosphatidylglycerol (DMPG), exhibited SANS profiles consistent with a perforated lamellar morphology for the magnetically alignable phase. Correspondingly, F68 diffusion in this magnetically aligned phase was normal Gaussian, in that the mean square displacements increased linearly with the experimental diffusion time, with a lateral diffusion coefficient of $1.9 \times 10^{-11} \text{ m}^2 \text{ s}^{-1}$ consistent with a lipid bilayer inserted configuration. Neutral bicellar mixtures, that is, lacking DMPG, in contrast, displayed SANS profiles characteristic of ribbons arranged in such a fashion as to produce extended lamellae. Within the lamellae, the ribbons exhibited an in-plane periodicity (interribbon) of between 120 and 140 Å. Correspondingly, F68 diffusion was non-Gaussian, exhibiting a square root diffusion time dependence of the mean square displacement indicative of one-dimensional curvilinear diffusion. The presence or absence of DMPG, rather than of F68, dictated the ribbon versus lamellar morphology, with F68 reflecting this difference via its lateral diffusion behavior. Although ribbons have been reported previously, this is the first study to show that they aggregate, most likely into extended lamellar sheets, and eventually fold into multilamellar vesicles.

Introduction

The Pluronic family of triblock copolymers consist of a hydrophobic polypropylene oxide (PPO) central block flanked by hydrophilic polyethylene oxide (PEO) end blocks (see Figure 1). Pluronics have received particular attention of late because, in addition to their potential as drug delivery vehicles and their utility in encouraging drug uptake *in vitro*,^{1,2} they incorporate readily into lipid bilayers where they facilitate lipid flip-flop and transbilayer drug permeation.^{3,4} To understand the origin of these effects, Pluronic interactions with lipid bilayers and their effects on bilayer morphology have been studied using small-angle X-ray scattering (SAXS) and atomic force microscopy (AFM).^{5,6} Of particular importance is the relative size of the PPO and PEO segments: too short a hydrophobic PPO segment reduces affinity for lipid bilayers, while too lengthy a PPO segment favors self-association rather than bilayer incorporation. An outstanding issue is whether a given lipid-bilayer-associated Pluronic adopts a bilayer-spanning conformation or remains within one leaflet, where it adopts a U-shaped or V-shaped conformation. One means by which to address this question

would be to measure the lateral diffusion of a lipid-bilayer-associated Pluronic, in that rather different diffusion behavior might be exhibited for these two different conformations. In any case, we are not aware of any reports regarding the lateral diffusion of Pluronics.

Here we describe the first measurement of the lateral diffusion of a lipid-bilayer-associated Pluronic, specifically Pluronic F68, or simply F68 (Figure 1), which consists of 30 propylene oxide (PO) units capped on either end by 76 ethylene oxide (EO) units. The hydrophobic central PPO span is sufficiently long to traverse the hydrophobic core of a lipid bilayer. The hydrophilic PEO end-caps remain sequestered in the aqueous medium bathing the lipid bilayer. To measure its lateral diffusion coefficient, we incorporated F68 into magnetically aligned bicellar mixtures and applied the proton (¹H) stimulated echo (STE) pulsed field gradient (PFG) nuclear magnetic resonance (NMR) diffusion method introduced by Tanner.⁷

Bilayered micelles, or bicelles, are a model membrane system consisting of binary mixtures of short chain lipids, for example, 1,2-dihexanoyl-*sn*-glycero-3-phosphocholine (DHPC), and long chain lipids, for example, 1,2-dimyristoyl-*sn*-glycero-3-phosphocholine (DMPC).⁸ The long chain lipids assemble into a planar bilayer, while the short chain lipids segregate to edge regions of high curvature. The resulting single-bilayer-thickness self-assemblies exhibit macroscopic morphologies that vary with increasing DMPC/DHPC ratio in the bicellar mixture, from disks to chiral nematic ribbons to lamellar sheets perforated by toroidal holes.^{9,10}

*To whom correspondence should be addressed. Telephone: 905 828 3805. Fax: 905 828 5425. E-mail: pm.macdonald@utoronto.ca.

(1) Kabanov, A. V.; Batrakova, E. V.; Alakhov, V. Y. *Adv. Drug Delivery Rev.* **2002**, *54*, 759–779.

(2) Kabanov, A. V.; Batrakova, E. V.; Miller, D. W. *Adv. Drug Delivery Rev.* **2003**, *55*, 151–164.

(3) Yaroslavov, A. A.; Melk-Nubarov, N. S.; Menger, F. M. *Acc. Chem. Res.* **2006**, *39*, 702–710.

(4) Demina, T.; Grozdova, I.; Krylova, O.; Zhirnov, A.; Istratov, V.; Frey, H.; Kautz, H.; Melik-Nubarov, N. *Biochemistry* **2005**, *44*, 4042–4054.

(5) Firestone, M. A.; Wolf, A. C.; Seifert, S. *Biomacromolecules* **2003**, *4*, 1539–1549.

(6) Liang, X. M.; Mao, G. Z.; Ng, K. Y. S. *J. Colloid Interface Sci.* **2005**, *285*, 360–372.

(7) Tanner, J. E. *J. Chem. Phys.* **1970**, *52*, 2523–2526.

(8) Sander, C. R.; Schwonek, J. P. *Biochemistry* **1992**, *31*, 8898–8905.

(9) Bolze, J.; Fujisawa, T.; Nagao, T.; Norisada, K.; Saito, H.; Naito, A. *Chem. Phys. Lett.* **2000**, *329*, 215–220.

(10) Nieh, M. P.; Glinka, C. J.; Krueger, S.; Prosser, R. S.; Katsaras, J. *Biophys. J.* **2002**, *82*, 2487–2498.

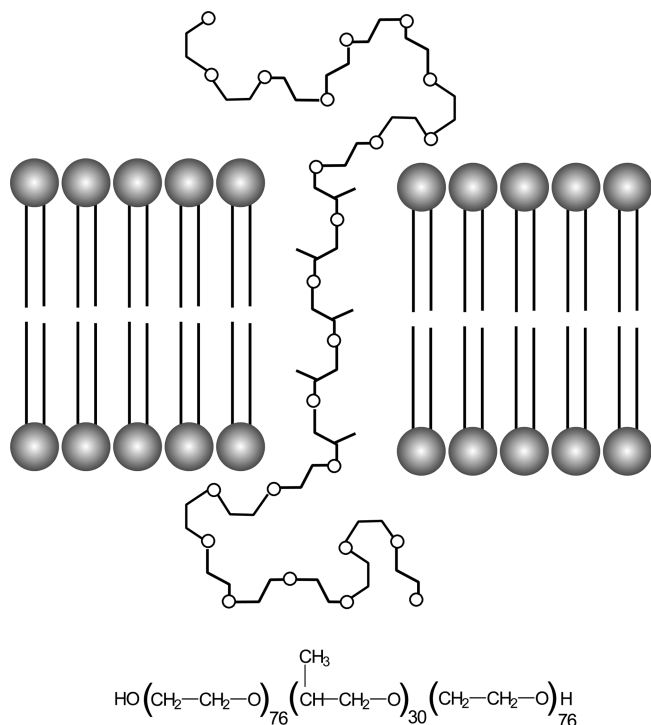


Figure 1. Molecular structure of Pluronic F68 and schematic of one possible conformation in a lipid-bilayer-bound state. The 30 propylene oxide units are sufficient to span a lipid bilayer.

Commonly, but not universally, it is the disk morphology which is being referred to when the term bicelle is employed in the literature. To avoid conflating composition with morphology, we will employ here the term bicellar mixture as embracing all bicellar morphologies in general.

Importantly, for PFG NMR diffusion studies, many bicellar mixtures spontaneously align in magnetic fields such that there is a narrow distribution of orientations of the bilayer normal with respect to the magnetic field direction. PFG NMR diffusion techniques then measure directly and readily the lateral diffusion of any lipid-bilayer-incorporated species, provided it yields an NMR-observable signal and that the gradients are applied perpendicular to the bilayer normal.^{11,12}

Because bicelle macroscopic morphology is relatively pliable and because Pluronics are known to be capable of influencing the lipid bilayer macroscopic phase state,¹³ we have performed parallel small-angle neutron scattering (SANS) measurements on bicellar mixtures incorporating Pluronic F68. As detailed in a recent review,¹⁴ and the original research cited therein, SANS measurements are especially suited to providing morphology information on “soft materials”, such as bicellar mixtures. A key finding of SANS studies is that, in addition to the disk and perforated lamellar morphologies, under certain circumstances, bicellar mixtures appear to adopt a chiral nematic phase consisting of DMPC-rich “ribbons” edged, presumably, with DHPC. Among other factors, the presence or absence of charged lipid within the bicellar mixtures appears to dictate whether the perforated lamellar or chiral nematic phase, respectively, predominates.

We examine here both neutral and negatively charged bicellar mixtures incorporating F68 using a combination of SANS to

define the macroscopic morphology and PFG NMR to define the diffusion behavior of F68. Our goals are to determine, first, whether the chiral nematic and the perforated lamellar phases are still observed when F68 is incorporated into bicellar mixtures, second, whether, and to what degree, F68 diffusion reflects these different morphological phases, and third, what can be deduced regarding the conformation of the bound Pluronic.

Experimental Section

Materials. DMPC (1,2-dimyristoyl-*sn*-glycero-3-phosphocholine), DHPC (1,2-dihexanoyl-*sn*-glycero-3-phosphocholine), and DMPG (1,2-dimyristoyl-*sn*-glycero-3-phosphoglycerol) were purchased from Avanti Polar Lipids, Alabaster, AL. Pluronic F68 was purchased from Sigma-Aldrich, Oakville, ON, Canada, as were all other biochemicals and reagents employed.

Bicelle Preparation. Neutral bicellar mixtures for SANS measurements were composed of DMPC/DHPC/F68 ([DMPC]/[DHPC] = 4.5 + 0.4 mol % F68 relative to DMPC) and were prepared to contain 20, 25, or 30 wt % lipid in D₂O solution (10 mM Tris, pH 7.4). Negatively charged bicellar mixtures contained in addition DMPG at 1 mol % relative to DMPC and were prepared to consist of 25 wt % lipid in D₂O solution. For PFG NMR measurements, all bicellar mixtures, both neutral and negatively charged, were composed of [DMPC]/[DHPC] = 4.5 and contained 25 wt % lipid in D₂O solution. A typical preparation procedure involved dissolving the desired quantities of DMPC, DHPC, DMPG, and F68 in the desired volume of D₂O solution, followed by several cycles of freezing, thawing, and gentle vortexing that were continued until a clear solution was obtained. The sample was then stored at 4 °C for up to 24 h before use.

For SANS measurements, the bicellar mixture was transferred into the sample holder (see below) at 4 °C and then placed directly into the neutron beam. For NMR measurements, the bicellar mixture was transferred into a 5 mm NMR sample tube at 4 °C and placed in the bore of a 300 MHz NMR spectrometer. The sample temperature was then raised to 30 °C. An annealing procedure was carried out involving repeated cycling of the temperature between 20 and 35 °C, with 10–15 min of equilibration at either extreme to encourage magnetic alignment. The quality of the magnetic alignment was assessed via ³¹P NMR spectroscopy. Once satisfactory magnetic alignment was obtained, the sample temperature was left at 30 °C.

Small-Angle Neutron Scattering. Small-angle neutron scattering measurements were conducted on the recently modified N5 spectrometer located at the National Research Universal (NRU) reactor (Chalk River, Ontario, Canada).¹⁵ Neutrons of 2.37 Å were chosen using a pyrolytic graphite (PG) monochromator. A converging Soller collimator was used to enhance neutron flux on the samples by a factor of 20, while higher-order neutron wavelengths (e.g., $\lambda/2$, $\lambda/3$, etc.) were selected out with a PG filter.¹⁵ Scattered intensity was measured as a function of scattering angle θ by a ³He position-sensitive, multiwire detector. The data were corrected using transmission and empty cell measurements over the same range of θ as in the case with sample. Reduced SANS data are presented as a function of scattering vector q (between 0.015 and 0.3 Å⁻¹), defined as

$$q = \frac{4\pi}{\lambda} \sin\left(\frac{\theta}{2}\right) \quad (1)$$

Individual samples were loaded in quartz cells with a path length of 2 mm, which were then placed and secured in a temperature controlled aluminum sample holder. For a given temperature, each sample was equilibrated for at least 20 min.

(11) Soong, R.; Macdonald, P. M. *Biophys. J.* **2005**, *88*, 255–268.

(12) Soong, R.; Macdonald, P. M. *Biophys. J.* **2005**, *89*, 1850–1860.

(13) Bergstrand, N.; Edwards, K. J. *Colloid Interface Sci.* **2004**, *276*, 400–407.

(14) Katsaras, J.; Harroun, T. A.; Pencer, J.; Nieh, M.-P. *Naturwissenschaften* **2005**, *92*, 355–366.

(15) Nieh, M.-P.; Yamani, Z.; Kučerka, N.; Katsaras, J.; Burgess, D.; Breton, H. *Rev. Sci. Instrum.* **2008**, *79*, 095102.

SANS data obtained from the various samples contain between 0 and 2 quasi-Bragg reflections sitting on a background with two monotonic decays; the absolute value of the slope at high q is greater than that at low q . As a result, we used the following phenomenological equation to generate the two decays and the requisite Gaussians to fit the data:

$$I(q) = \frac{s_0}{(1 + s_1 q^m + s_2 q^n)} + p_1 \exp\left[\frac{-(q - q_1)^2}{\sigma_1^2}\right] + p_2 \exp\left[\frac{-(q - q_2)^2}{\sigma_2^2}\right] + \text{BGD} \quad (2)$$

where the first term describes slope behavior ($-m$ and $-n$), with coefficients s_0 , s_1 , and s_2 used to adjust their ratios. The two Gaussians appear in the second and third terms with coefficients p_1 and p_2 . Their positions and widths are defined by q_1 and q_2 , and σ_1 and σ_2 , respectively. BGD is the term used to describe the incoherent background. The main purpose of this phenomenological equation is to determine the positions and widths of the Gaussians.

NMR Spectroscopy. All NMR spectra were recorded on a Chemagnetics (Fort Collins, CO) CMX300 NMR spectrometer using a magnetic resonance imaging/spectroscopy probe (Doty Scientific, Columbia, SC) equipped with actively shielded gradient coils and dual radio frequency channels, in addition to the lock channel. The NMR spectra of the various magnetically aligned samples at 30 °C consist of relatively narrow resonances spreading over a relatively narrow spectral range, such that they could be acquired under solution state NMR conditions.

³¹P NMR spectra were recorded at 121.6 MHz using a Hahn echo pulse scheme, with quadrature detection, complete phase cycling of the pulses, and proton decoupling during signal acquisition. Typical acquisition parameters were as follows: a 90° pulse length of 25 μs, an echo delay of 50 μs, a recycle delay of 3 s, a spectral width of 100 kHz, and a 1K data size. The spectra were processed with an exponential multiplication equivalent to 50 Hz line broadening prior to Fourier transformation and were referenced to 85% phosphoric acid.

Lateral diffusion coefficients were measured using the STE PFG ¹H NMR sequence,⁷ with phase cycling of the radio frequency pulses to remove unwanted echos.¹⁶ Typical acquisition parameters were as follows: a 90° pulse length of 50 μs, a recycle delay of 5 s, a spectral width of 10 kHz, and a 2K data size. The first, or spin echo, delay was typically 10 ms in duration, while the second, or stimulated echo, delay was varied from 200 up to 800 ms. The gradient pulse duration was incremented in 12 steps up to a maximum of 6 ms duration. The gradient pulse amplitude (typically 250 G cm⁻¹) was calibrated using the known diffusion coefficient of HDO at 25 °C.¹⁷ Spectra were processed with an exponential multiplication equivalent to 5 Hz line broadening prior to Fourier transformation and were referenced to external tetramethylsilane.

Results and Discussion

Morphology of Neutral versus Charged F68-Containing Bicellar Mixtures from SANS. Figure 2 shows the temperature-dependence of SANS intensity versus q plots for 20 wt % neutral bicellar mixtures, that is, lacking DMPG, but containing 0.4 mol % F68. Nearly identical structural changes as a function of temperature were observed for 20, 25, and 30 wt % lipid, so we first focus attention solely on the 20 wt % lipid mixtures.

At 295 K, SANS intensities at low q remain constant, but decay monotonically at higher q in a manner reminiscent of neutral

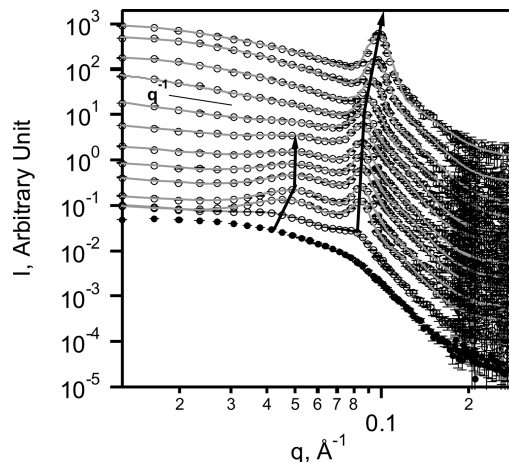


Figure 2. SANS results on neutral DMPC/DHPC/F68 bicellar mixtures in D₂O solution (total lipid concentration = 20 wt %) at a series of temperatures (i.e., 294.5, 298.5, 300, 301.9, 303.5, 305, 306.7, 308, 309.7, 311.2, 312.8, 314.4, and 318.6 K, from bottom to top). The data were rescaled for clarity. The solid symbols are data from the bicellar phase, and the gray lines are the best fits to the data using eq 2. The two lines show the movement of the two quasi-Bragg peaks as a function of temperature.

bicellar mixtures in the absence of F68.^{10,14,18} At 298.5 K, two quasi-Bragg peaks are apparent, at $q_1 \sim 0.04 \text{ \AA}^{-1}$ and $q_2 \sim 0.08 \text{ \AA}^{-1}$, which have been observed previously, but whose origin has not been elaborated fully.^{10,14,19–21} The fact that the width σ_1 of the low q peak is approximately 10 times greater than σ_2 , at high q , implies that the two peaks originate from in-plane (broad peak) and out-of-plane (sharp peak) structures contained within the same structure.²² The presence of two peaks is most obvious between 300 and 303 K and persists until 308 K. Once the temperature is increased above 310 K, only the sharp peak is observed at $\sim 0.095 \text{ \AA}^{-1}$, corresponding to a repeat spacing usually associated with pure DMPC multilamellar vesicles (MLVs).^{10,14,18,20,21} It should be noted that neutral DMPC/DHPC mixtures exhibit their strongest tendency to align magnetically between 298.5 and 308 K. At such temperatures, various structures have been proposed including bicelle disks,^{8,23,24} bilayered ribbons,^{14,20,21} and perforated lamellae.^{10,25} To determine the morphology at this intermediate temperature range, we used eq 1 to obtain the particular peak positions (q_1 and q_2) and peak widths (σ_1 and σ_2). The best fit results for DMPC/DHPC/F68 mixtures at all three wt % lipid samples as a function of temperature are summarized in Table 1.

Characteristic lengths d_i (calculated from $2\pi/q_i$) are shown in Figure 3 for both the low q broad peak d_1 and the high q narrow peak d_2 as a function of temperature. For the low q broad peak, the value of d_1 drops abruptly between 298.5 K and 300 K and then remains approximately constant at roughly 120 Å as the

(18) Nieh, M.-P.; Glinka, C. J.; Krueger, S.; Prosser, R. S.; Katsaras, J. *Langmuir* **2001**, *17*, 2629–2638.

(19) Katsaras, J.; Tristram-Nagle, S.; Liu, Y.; Headrick, R. L.; Fontes, E.; Mason, P. C.; Nagle, J. F. *Phys. Rev. E* **2000**, *61*, 5668–5677.

(20) Nieh, M.-P.; Raghunathan, V. A.; Glinka, C. J.; Harroun, T. A.; Pabst, G.; Katsaras, J. *Langmuir* **2004**, *20*, 7893–7897.

(21) Harroun, T. A.; Koslowsky, M.; Nieh, M.-P.; de Lannoy, C.-F.; Raghunathan, V. A.; Katsaras, J. *Langmuir* **2005**, *21*, 5356–5361.

(22) Katsaras, J.; Raghunathan, V. A.; Dufourc, E. J.; Dufourcq, J. *Biochemistry* **1995**, *34*, 4684–4688.

(23) Sanders, C. R., II; Hare, B. J.; Howard, K. P.; Prestegard, J. H. *Prog. NMR Spectrosc.* **1994**, *26*, 421–444.

(24) Vold, R. R.; Prosser, R. S. *J. Magn. Reson. B* **1996**, *113*, 267–271.

(25) van Dam, L.; Karlsson, G.; Edwards, K. *Biochim. Biophys. Acta, Biomembr.* **2004**, *1664*, 241–256.

(16) Fauth, J.-M.; Schweiger, A.; Braunschweiler, L.; Forrer, J.; Ernst, R. R. *J. Magn. Reson.* **1986**, *66*, 74–85.

(17) Mills, R. *J. Phys. Chem.* **1973**, *77*, 685–688.

Table 1. Best Fit Peak Positions and Widths from SANS Data of 20, 25, and 30 wt % DMPC/DHPC/F68 (Neutral) and 25 wt % DMPC/DHPC/DMPG/F68 (Charged) Bicellar Mixtures^a

T (K)	neutral						charged	
	20 wt %		25 wt %		30 wt %		25 wt %	
	q_1/σ_1	q_2/σ_2	q_1/σ_1	q_2/σ_2	q_1/σ_1	q_2/σ_2	1st order/ σ_1	2nd order/ σ_2
298.5	0.040/0.009	0.080/0.0037	0.044/0.019	0.084/0.0017	0.043/0.008	0.084/0.0015	—	—
300	0.047/0.011	0.081/0.0012	0.049/0.018	0.088/0.0014	0.048/0.012	0.085/0.0012	—	—
301.9	0.050/0.012	0.084/0.0012	0.051/0.017	0.088/0.0013	0.050/0.018	0.087/0.0014	—	—
302.2	—	—	—	—	—	—	0.054/0.013	—
303.5	0.051/0.013	0.084/0.0012	0.051/0.024	0.088/0.0013	0.051/0.019	0.088/0.0014	—	—
305	0.051/0.014	0.084/0.0012	0.050/0.026	0.091/0.0014	0.051/0.020	0.088/0.0015	—	—
306.7	0.050/0.012	0.084/0.0013	0.048/0.029	0.091/0.0014	0.051/0.022	0.088/0.0015	0.052/0.0013	0.109/0.0012
308	0.050/0.010	0.084/0.0013	—	0.091/0.0013	0.051/0.023	0.088/0.0016	—	—
309.7	—	0.084/0.0014	—	0.091/0.0013	0.051/0.017	0.088/0.0015	—	—
310.5	—	—	—	—	—	—	0.052/0.0013	0.108/0.0018
311.2	—	0.089/0.0024	—	0.094/0.0013	—	0.091/0.0014	—	—
312.8	—	0.092/0.0013	—	0.095/0.0011	—	0.095/0.0014	0.051/0.0013	0.105/0.0016
318.6	—	0.098/0.0014	—	0.098/0.0011	—	0.098/0.0014	0.051/0.0012	0.105/0.0015

^aThe uncertainties in peak positions and peak widths for ribbon correlation are less than ± 0.003 and ± 0.002 , and for lamellar correlations are less than ± 0.002 and ± 0.0005 , respectively.

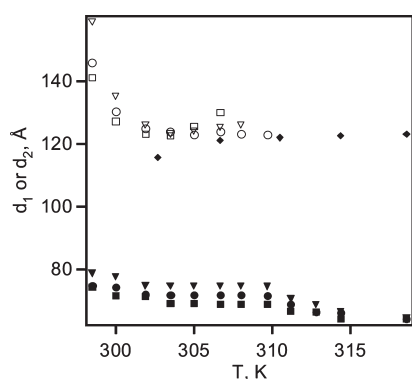


Figure 3. Values of the d -spacings as determined from SANS data of 30 wt % (circles), 25 wt % (squares), and 20 wt % (triangles) DMPC/DHPC/F68 bicellar mixtures, as well as from 25 wt % bicellar mixtures doped with 1 mol % DMPG (tilted squares), as a function of temperature. Solid symbols represent the lamellar spacings, while the open symbols represent spacings between the ribbons.

temperature is increased to 308 K. The fact that the σ_1 values are relatively large (0.009 – 0.014 \AA^{-1}) indicates that the variations in d_1 are rather significant.

Similar observations reported previously for otherwise identical DMPC/DHPC bicellar mixtures, but lacking F68, over this same range of temperatures, were interpreted as arising from a ribbonlike morphology.^{14,20,21,25} Hence, the in-plane characteristic length d_1 would correspond to the average in-plane spacing between individual ribbons. If this is the case, it also makes sense that the correlation length is small, giving rise to a broad peak. Further evidence supporting the ribbon morphology is that the slope at low q decays as q^{-1} , a property characteristic of long one-dimensional objects. For homogeneously dispersed ribbons, d_1 is expected to scale as (lipid concentration)^{-1/2}, due to two-dimensional swelling. However, as Figure 3 demonstrates, d_1 does not change as a function of lipid concentration, indicating that the ribbons do not freely swell, implying that they are somehow constrained, possibly through being interconnected. As temperature is increased beyond 308 K, the low q peak associated with the correlation between ribbons disappears, while the q^{-1} decay remains unaltered (persisting up to 311 K in the case of 30 wt %), indicating that, although ribbons are still present, they are no longer correlated.

The high q sharp peak (σ_2 ranged from 0.001 to 0.002 \AA^{-1}) represents a smectic phase, most likely similar to the lamellar phase reported previously.^{14,26} Between 300 and 310 K, the assumed lamellar repeat spacing d_2 exhibits practically no temperature-dependence ($d_2 > 68 \text{ \AA}$) and then drops to the nominal value of 64 \AA (the lamellar spacing of pure DMPC MLVs in water²⁷) for all samples above 314 K (Figure 3). Furthermore, these mixtures turn cloudy, behavior typical of MLVs, at temperatures $\geq 314 \text{ K}$. The variation of the assumed lamellar spacing d_2 suggests that the intermediate temperature morphology, which is magnetically alignable, is different from MLVs that do not magnetically align. Figure 3 also shows that, unlike lamellae doped with a charged lipid,^{10,18} where the lamellar spacing increases linearly with decreasing lipid concentration, the swelling ability of this neutral DMPC/DHPC/F68 mixture is somewhat limited, swelling only a few Ångstroms, that is, from 68 to 75 \AA , when diluted from 30 to 20 wt %. This behavior is consistent with that observed in long-chain zwitterionic phospholipid bilayers.^{28,29}

In light of the aforementioned analysis, we propose the coexistence of ribbons and lamellae in neutral bicellar mixtures containing F68 at temperatures where magnetic alignment occurs. The question is whether these structures coexist as two independent domains or are somehow forming one morphology. The simultaneous appearance of the two quasi-Bragg peaks, and the fact that they do not change much with swelling, seems to imply the latter scenario. Based on SANS and NMR diffusion data (see below), we propose the following morphologies, shown schematically in Figure 4. As previously reported,^{10,18} at temperatures below the main transition temperature of DMPC ($T < T_m^{\text{DMPC}} \sim 296 \text{ K}$), bicellar disks composed of DMPC and DHPC coalesce, as a function of increasing temperature, into wormlike ribbons due to the increased line tension resulting from the loss of DHPC into solution from the edge of the bilayered micelle. At this stage, the ribbons are not strongly correlated with each other; that is, no characteristic length between individual ribbons is observed. As temperature is increased, approaching and then exceeding the main transition temperature of DMPC ($T > T_m^{\text{DMPC}}$), DHPC becomes miscible with DMPC as both are now in the liquid crystalline (L_α) phase. This results in a further

(26) van Dam, L.; Karlsson, G.; Edwards, K. *Langmuir* **2006**, *22*, 3280–3285.

(27) Kučerka, N.; Nieh, M.-P.; Pencic, J.; Harroun, T. A.; Katsaras, J. *Curr. Opin. Colloid Interface Sci.* **2007**, *12*, 17–22.

(28) Katsaras, J.; Stinson, R. H. *Biophys. J.* **1990**, *57*, 649–655.

(29) Katsaras, J. *J. Phys. Chem.* **1995**, *99*, 4142–4147.

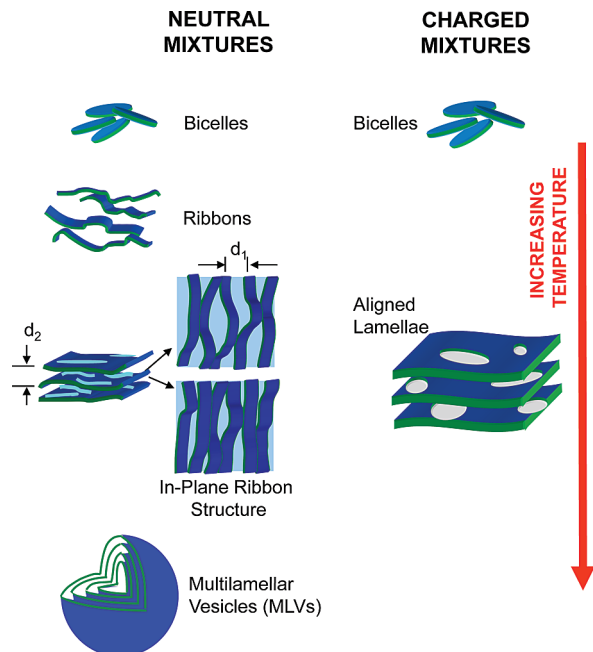


Figure 4. Schematic of the temperature-dependent morphology changes undergone by neutral (DMPC/DHPC/F68) and charged (DMPG/DMPC/DHPC/F68) bicellar mixtures as derived from SANS. In either case, at a temperature below the DMPC main phase transition, the morphology is discoidal. For neutral bicellar mixtures, the morphology evolves from ribbons to ribbons forming extended lamellae to multilamellar vesicles. For charged bicellar mixtures, the morphology is that of extended lamellae perforated by toroidal holes lined with DHPC.

loss of DHPC from the ribbon's edge, this time to the ribbon's DMPC-rich planar region. The ribbon's edge becomes unstable, causing individual ribbons to partially fuse, forming regions with extended lamellar sheets, while in places maintaining the ribbon morphology. The ribbon spacing (d_1) decreases, while the association between ribbons becomes more significant as a result of being confined within a lamellar sheet (a broad peak). Interestingly, *ribbon in-plane spacing is not affected by lipid concentration*. In fact, the cryo-transmission electron microscopy (cryo-TEM) images reported by van Dam et al.²⁵ showed a similar ribbon spacing (100–150 Å) even at a much lower lipid concentration (3 wt %) for [DMPC]/[DHPC] ratios of between 2.5 and 4. The fact that the samples turn translucent implies that the ribbon–lamellar morphology has dimensions of the order of the wavelength of visible light. Finally, since the sample becomes opaque upon further increasing the temperature, the lamellae eventually form MLVs as a result of further DHPC migration into the planar region.

When doped with a charged lipid such as DMPG, DMPC/DHPC bicellar mixtures have been found to align better and remain stable over a wider range of temperatures^{30–32} than non-DMPG-doped mixtures. To determine whether F68 influences this effect of DMPG, we studied the structure of DMPC/DHPC/F68 mixtures ([DMPC]/[DHPC] = 3.5 and 0.4 mol % of F68) doped with 1 mol % DMPG. The SANS intensity versus q plots of such mixtures at 25 wt % lipid are shown in Figure 5 as a function of temperature. Although the SANS data of the DMPG-doped

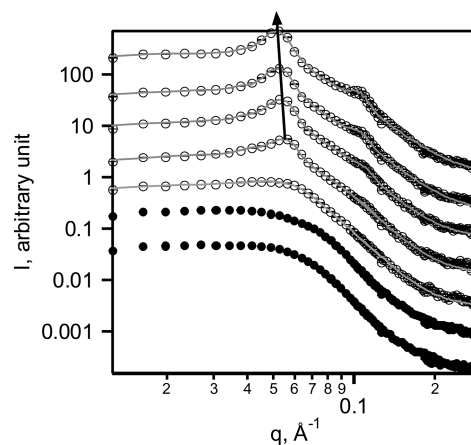


Figure 5. SANS results of negatively charged DMPG/DMPC/DHPC/F68 bicellar mixtures in D_2O solution (total lipid concentration = 25 wt %) at a series of temperatures (i.e., 294.5, 302.7, 306.7, 310.5, 314.4, and 318.6 K, from bottom to top). The data were rescaled for clarity. The solid symbols are data from the bicellar phase, and the gray lines are the best fits to the data using eq 2. The line shows the movement of the quasi-Bragg lamellar peaks as a function of temperature.

sample at low temperatures resemble those of the non-DMPG-doped sample (presumably both form bicelle disks), there are significant differences between the scattering profiles observed for neutral and charged mixtures at higher temperatures. Specifically, in the presence of DMPG, the dominant feature is a narrow quasi-Bragg peak at $q \sim 0.051 \text{ \AA}^{-1}$ which exhibits a noticeable second order quasi-Bragg peak and shifts toward lower q with increasing temperature (see Table 1). This is interpreted as arising from the lamellar repeat distance which will be far larger in charged relative to neutral lamellae. In fact, the lamellar spacings of such charged bicellar mixtures have been reported to scale as [lipid concentration]⁻¹, up to 10 wt %.¹⁰ As shown in Figure 3, this lamellar repeat spacing increases with increasing temperature, most likely due to the continuous loss of DHPC from curved regions toward planar regions, which reduces the number and/or size of the perforations, thus increasing the “effective” area of the lamellae. Finally, the lamellar phase of the DMPG-doped mixture extends to higher temperatures without forming MLVs, consistent with the less opaque appearance of the sample (i.e., no formation of large lamellar domains of micrometer size heterogeneously distributed in the sample) and our previous reports.^{10,20}

A further significant difference is that there is no evidence of ribbons, in that the low q scattering intensity is q -independent, as opposed to the q^{-1} -dependence in non-DMPG-doped mixtures. Moreover, the lamellar phase of the DMPG-doped system ($T \geq 303 \text{ K}$) differs from that of the non-DMPG-doped system in that there is no broad peak associated with the interribbon spacing. The likely morphology, therefore, is that of extended lamellar regions perforated by DHPC-lined toroids, as shown schematically in Figure 4. However, due to the presence of the strong Bragg peak at $q \sim 0.051 \text{ \AA}^{-1}$, we cannot rule out the presence of ribbons entirely. In fact, ribbons have been observed previously in DMPG-doped mixtures with cryo-TEM.²⁶ Cryo-TEM images have also shown that such DMPG-doped and non-DMPG-doped samples are different,^{25,26} although their differences were not explicitly described.

In summary, SANS data indicate that, while the lamellae of non-DMPG-doped bicellar mixtures containing F68 are likely made up of interconnected ribbons, those of DMPG-doped bicellar mixtures are most likely perforated by DHPC-rich

(30) Crowell, K. J.; Macdonald, P. M. *Biochim. Biophys. Acta, Biomembr.* **1999**, *1416*, 21–30.

(31) Vold, R. R.; Whiles, J. A.; Struppe, J. *Biophys. J.* **2000**, *78*, 281–289.

(32) Nieh, M.-P.; Raghunathan, V. A.; Wang, H.; Katsaras, J. *Langmuir* **2003**, *19*, 6936–6941.

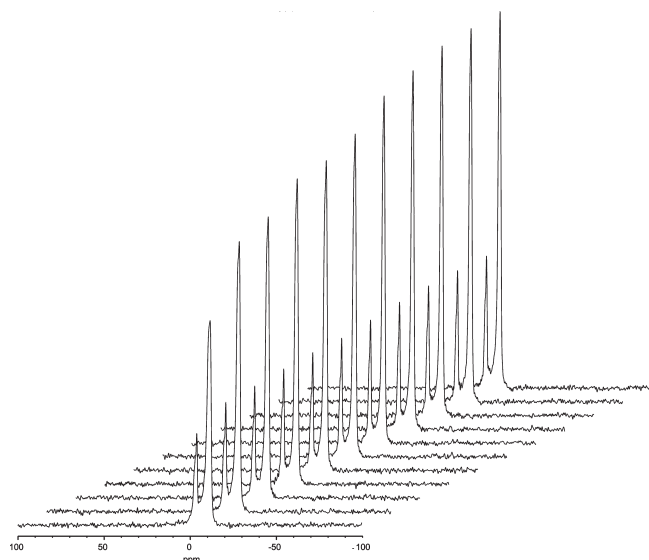


Figure 6. ^{31}P NMR spectra of magnetically aligned [DMPC]/[DHPC] = 4.5 bicellar mixtures in D_2O solution (total lipid concentration = 25 wt %, 30 °C) incorporating 1 mol % DMPG and 0.4 mol % F68, obtained at 2 h intervals after placing the sample in the magnet.

toroidal holes. Similar conclusion were derived from SANS data on otherwise identical bicellar mixtures lacking F68.^{10,14,18} Thus, F68 is not the cause of these morphological differences, but instead surface charge appears to be the critical factor.

NMR Diffusion Measurements on Pluronic F68 in Magnetically Aligned Neutral and Negatively Charged Bicellar Mixtures. As a prerequisite to PFG NMR diffusion measurements, we examined the magnetic alignment of F68-containing bicellar mixtures via phosphorus (^{31}P) NMR spectroscopy, with a typical result being shown in Figure 6, where spectra were acquired over a span of 12 h after placing the bicellar mixture in the magnet of the NMR spectrometer. The ^{31}P NMR spectra consist of two well-resolved, narrow resonances as is characteristic of magnetically aligned lipid bilayers having a narrow distribution of orientations of their bilayer normals relative to the direction of the external magnetic field.^{8,9} The more intense lower-frequency resonance at -12.4 ppm was assigned to DMPC, while the less intense higher-frequency resonance at -4.8 ppm was assigned to DHPC. The ratio of their integrated intensities was approximately 4.5, as expected based on their assignments. No separate DMPG ^{31}P NMR resonance could be resolved when DMPG was present due to the small quantity added (1 mol %), with the chemical shifts of DMPC and DHPC being virtually identical \pm DMPG. These chemical shifts are similar to those observed for otherwise identical bicellar mixtures without F68. Hence, the presence of 0.4 mol % F68 does not alter the spontaneous magnetic orientation of these self-assemblies which in this case leaves their bilayer normals oriented perpendicular to the magnetic field direction, a situation referred to as negative magnetic alignment. Over time, the line widths narrowed somewhat, but the precise chemical shifts remained constant. Importantly, there was no evidence of micellized DMPC or DHPC such as would produce a resonance at 0 ppm. We conclude that magnetically oriented bicellar mixtures containing F68 are suitable for NMR diffusion measurements.

Figure 7 shows a series of ^1H STE PFG NMR spectra of magnetically oriented [DMPC]/[DHPC] = 4.5 containing 0.4 mol % F68 as a function of the gradient pulse duration δ in the STE PFG NMR sequence. Three well-resolved resonances are evident

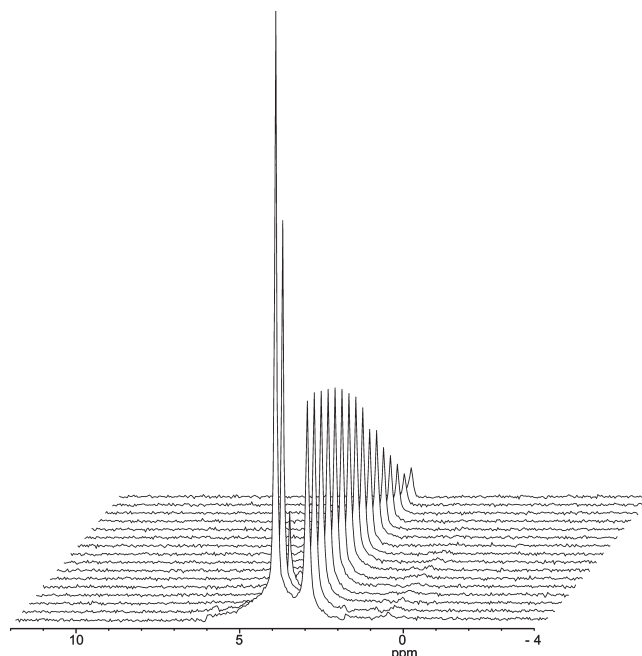


Figure 7. STE PFG ^1H NMR spectra of magnetically aligned [DMPC]/[DHPC] = 4.5 in D_2O solution (total lipid concentration = 25 wt %, 30 °C) incorporating 1 mol % DMPG and 0.4 mol % F68, as a function of increasing gradient pulse duration δ ($g = 266 \text{ G cm}^{-1}$, $\Delta = 400 \text{ ms}$).

at 4.2, 3.3, and 0.66 ppm, and are assigned to HDO, F68 ethylene oxide (EO) methylenes, and F68 propylene oxide (PO) methyls, respectively. Other expected resonances are largely absent due to their rapid relaxation relative to the delays present in the STE PFG NMR sequence. Qualitatively, in Figure 7, the HDO resonance decays rapidly with increasing δ , reflecting its rapid diffusion, while the two F68 resonances decay far more slowly, as expected for the slower diffusion of such a large molecule anchored within a lipid bilayer.

Quantitatively, in the STE PFG NMR diffusion experiment for the case of isotropic diffusion, the echo attenuation is Gaussian,⁷

$$E(k, \Delta) = \exp(-D\Delta k^2) \quad (3)$$

where D is the diffusion coefficient, Δ is the experimental diffusion time corresponding to the delay between the two field gradient pulses, and $k = \gamma\delta g$, where γ is the magnetogyric ratio, δ is the gradient pulse duration, and g is the gradient pulse amplitude. Equation 3 is valid within the short gradient pulse limit ($\delta \ll \Delta$) and ignores relaxation effects during the longitudinal and transverse echo delays in the STE sequence. The diffusion coefficient is extracted from the slope in a semilogarithmic plot of $E(k, \Delta)$ versus $k^2\Delta$ which should yield a straight line for a simple Gaussian diffusion behavior.

For a molecule incorporated into a lipid bilayer, the diffusion is anisotropic and is characterized by a diffusion tensor having tensor elements D_{\perp} and D_{\parallel} corresponding, respectively, to diffusion perpendicular and parallel to the bilayer normal. Thus, D_{\perp} is the lateral diffusion coefficient within the bilayer. For gradient pulses applied along the z -direction parallel to the main magnetic field, the apparent diffusion coefficient D_{zz} is

$$D_{zz} = \cos^2\theta D_{\parallel} + \sin^2\theta D_{\perp} \quad (4)$$

where θ is the polar angle between the bilayer normal and the direction of the applied field gradient.^{33,34} For the negatively

(33) Callaghan, P. T.; Söderman, O. *J. Phys. Chem.* **1983**, *87*, 1737–1744.

(34) Lindblom, G.; Orådd, G. *Prog. NMR Spectrosc.* **1994**, *26*, 483–515.

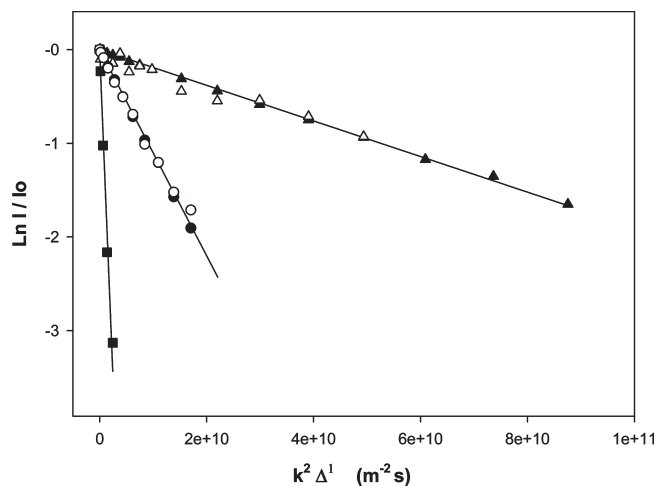


Figure 8. STE PFG ^1H NMR echo attenuations for F68 free in solution (circles) versus incorporated at 0.4 mol % into magnetically aligned [DMPC]/[DHPC] = 4.5, 25 wt %, 30 °C, bicellar mixtures containing 1 mol % DMPG (triangles). Closed symbols: EO resonance. Open symbols: PO resonance. Squares show the echo attenuation of water in the same bicellar mixtures.

magnetically aligned bicellar mixtures examined here, the bilayer normal is oriented uniformly at 90° relative to the magnetic field direction, so that the cosine term in eq 4 disappears and $D_{zz} = D_\perp$ such that we measure directly the molecule's lateral diffusion coefficient.

Figure 8 shows the diffusive decays obtained for F68 incorporated into bicellar mixtures containing 1 mol % DMPG versus free in aqueous solution. That of water within the same mixture is shown as well. The diffusive decays are clearly linear in all cases. For Pluronic F68, identical behavior is observed whether one monitors the EO methylene resonance or the PO methyl resonance, as one would expect. The particular diffusion coefficient is obtained from the slope in such a semilogarithmic plot.

For water in these bicellar mixtures, the diffusion coefficient was $1.4 \times 10^{-9} \text{ m}^2 \text{ s}^{-1}$, representing an approximately 30% reduction relative to that of free water at the same temperature.¹⁷ This is in accord with previous findings³⁵ and is attributed to a fraction of bound water at the polar lipid bilayer interface in fast exchange with bulk water in the interstices between adjacent bicelles.

The diffusion coefficient of F68 in aqueous solution was measured at 30 °C and a concentration of 1 wt %. Since the critical micelle concentration for Pluronic F68 is greater than 10 wt % at 30 °C,³⁶ we expect that under our conditions F68 is monomeric. The measured diffusion coefficient of $1.1 \times 10^{-10} \text{ m}^2 \text{ s}^{-1}$, which equates to a hydrodynamic radius of 2.53 nm via the Stokes–Einstein equation, confirms this expectation, since this hydrodynamic radius agrees with previous reports for monomeric F68, while micelles are far larger and diffuse far more slowly.³⁷ Nevertheless, this is somewhat faster diffusion and a somewhat smaller hydrodynamic radius than would be predicted for a comparably sized PEG chain in aqueous solution (ref 38 and references therein), suggesting that the hydrophobic PPO center block produces an overall structural compaction as it seeks to avoid the solvent water.

The diffusion coefficient of F68 mixed with charged bicellar mixtures is $1.8 \times 10^{-11} \text{ m}^2 \text{ s}^{-1}$, that is, roughly 1 order of

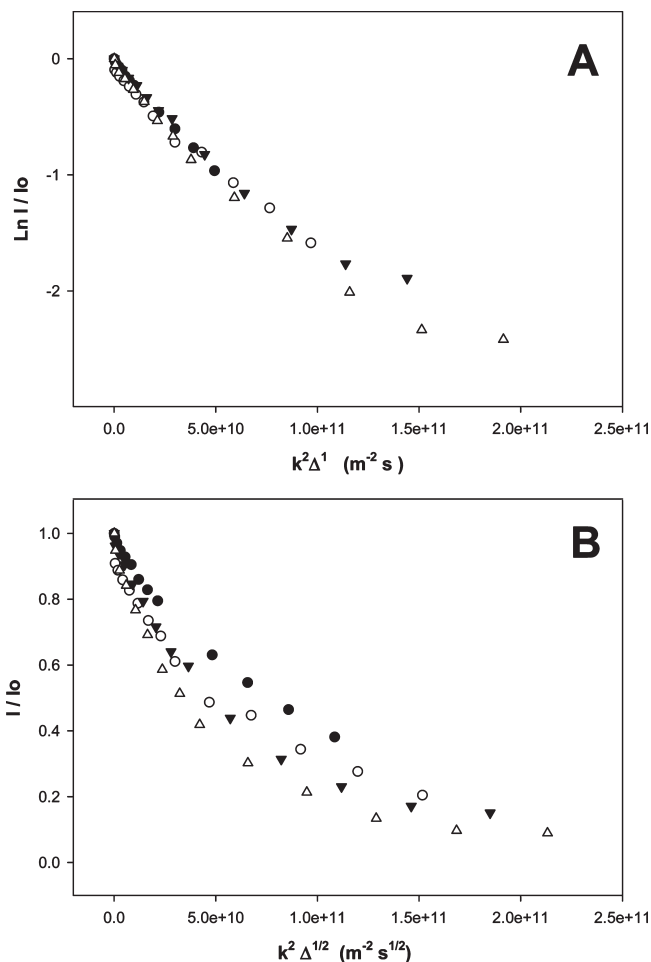


Figure 9. (A) Semilogarithmic plot of normalized stimulated echo intensity decays versus $k^2 \Delta$ for different diffusion times Δ in the case of the F68 EO resonance, as obtained from STE PFG ^1H NMR spectra (30 °C) of magnetically aligned [DMPC]/[DHPC] = 4.5, 25 wt % lipid, bicellar mixtures containing 1 mol % DMPG plus 0.4 mol % F68. For normal Gaussian diffusion, such plots should be linear and should overlap for different diffusion times. The diffusion coefficient is then obtained from the slope as per eq 3. $\Delta = 210$ ms (closed circles), 410 ms (open circles), 610 ms (closed triangles), and 810 ms (open triangles). (B) Normalized echo intensity decays versus $k^2 \Delta^{1/2}$ for the same data as (A). For curvilinear, that is, non-Gaussian, diffusion, such decays for different diffusion times would overlap.

magnitude slower diffusion than that found in aqueous solution, but rather similar, in fact, to that of PEG-ylated DMPC present in bicelles,¹¹ which strongly suggests that indeed F68 has associated with and been incorporated into the bicelles. Note that this slower diffusion cannot be due to mere trapping of aqueous F68 within the aqueous interstices between adjacent bicelles. Specifically, diffusion studies of comparably sized PEGs present in the interstices of comparable bicelles demonstrate that strong confinement effects commence only once $R_g/H > 0.4$, where R_g is the polymer's radius of gyration and $H \sim 60 \text{ \AA}$ is the spacing between adjacent bicelle surfaces under our conditions.³⁸ Thus, confinement effects alone cannot reduce by 1 order of magnitude the diffusion coefficient of F68 where the radius of hydration equals 25 Å.

For normal Gaussian diffusion, a semilogarithmic plot of $E(k, \Delta)$ versus $k^2 \Delta$ will be linear and will overlap for different diffusion times Δ . As shown in Figure 9, this is the case for F68 in negatively charged bicellar mixtures when the EO resonance is

(35) Soong, R.; Macdonald, P. M. *Langmuir* **2009**, *25*, 380–390.

(36) Kabanov, A.; Nazarova, I.; Astafieva, I.; Batrkova, E.; Alakhov, V.; Yaroslavov, A.; Kabanov, V. *Macromolecules* **1995**, *28*, 2303–2314.

(37) Zhou, Z.; Chu, B. J. *Colloid Interface Sci.* **1988**, *126*, 171–180.

(38) Soong, R.; Macdonald, P. M. *Langmuir* **2008**, *24*, 518–527.

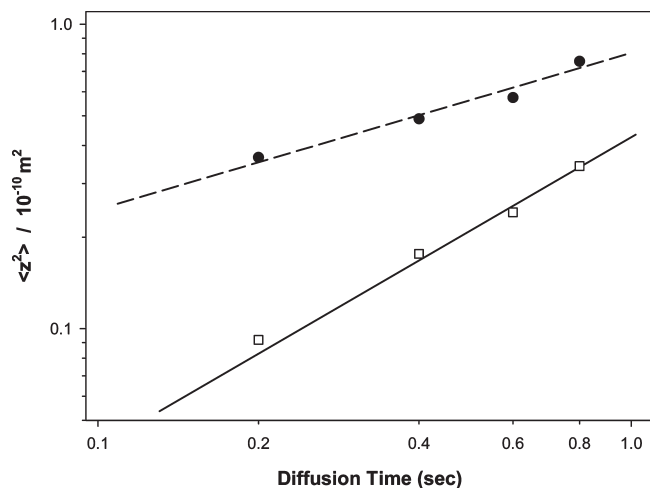


Figure 10. Log–log plot of the mean square displacement $\langle z^2 \rangle$ versus diffusion time Δ for F68 in negatively charged bicellar mixtures containing 1 mol % DMPG (open squares) and neutral bicellar mixtures (closed circles) lacking DMPG. $\langle z^2 \rangle$ was calculated using eq 6.

monitored. (The PO resonance is too weak to permit reliable quantification at all diffusion times). There is some slight curvature apparent at higher values of $k^2\Delta$, but only when the intensity has fallen to less than 5% of its initial value and where signal-to-noise has become an issue for purposes of quantification, as evident from the increased scatter in the data. Otherwise, the diffusion of F68 appears to be unrestricted over a length scale corresponding to the root-mean-square (rms) displacement $\langle z^2 \rangle^{1/2}$. The rms displacement achieved over a particular diffusion time in the direction of the applied gradient is obtained from

$$\langle z^2 \rangle^{1/2} = [4D\Delta]^{1/2} \quad (5)$$

and is found to equal 7.6×10^{-6} m for the case of $\Delta = 800$ ms. This far exceeds the size of a discoidal bicelle as estimated from the “ideal bicelle” model³⁹ and indicates that, instead, these bicellar mixtures have assumed a lamellar morphology capable of sustaining unrestricted diffusion over such distances. This interpretation conforms with phase diagrams obtained by SANS for bicellar mixtures containing the negatively charged lipid DMPG^{10,14} and with the SANS data presented above for negatively charged bicellar mixtures incorporating F68. Further to this point, in the limit of small k , one finds

$$E(k, \Delta) = 1 - \frac{\langle z^2 \rangle k^2}{2} \quad (6)$$

so that the mean square displacement may be evaluated from the initial slope of $E(k, \Delta)$ when plotted as a function of k^2 . The mean square displacements obtained in this way for different diffusion times Δ are plotted in a log–log fashion in Figure 10. For normal Gaussian diffusion, $\langle z^2 \rangle \propto \Delta$, and this direct dependence on diffusion time is evident in Figure 10 for the case of F68 in bicellar mixtures containing 1 mol % DMPG.

In contrast, for the case of neutral bicellar mixtures, that is, in the absence of DMPG, the diffusion of F68 is distinctly non-Gaussian. As shown in Figure 11A, a semilogarithmic plot of $E(k, \Delta)$ versus $k^2\Delta$ is obviously nonlinear, while diffusive decays obtained for different diffusion times $200 \text{ ms} < \Delta < 600 \text{ ms}$ fail to overlap. When

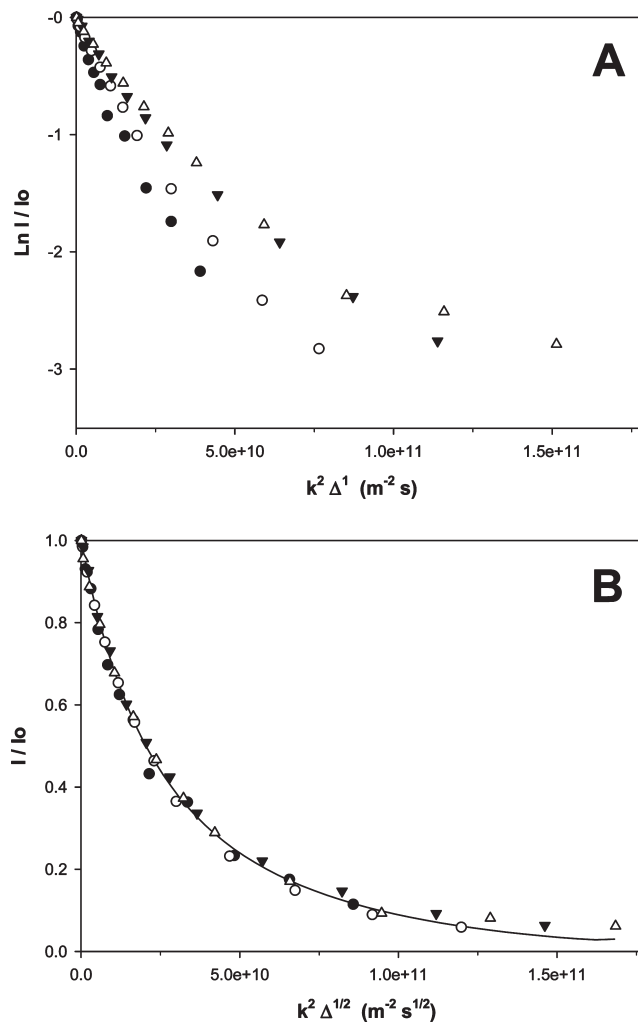


Figure 11. (A) Semilogarithmic plot of normalized stimulated echo intensity decays versus $k^2\Delta$ for different diffusion times Δ in the case of the F68 EO resonance, as obtained from STE PFG ^1H NMR spectra (30 °C) of magnetically aligned [DMPC]/[DHPC] = 4.5, 25 wt % lipid, neutral bicellar mixtures containing 0.4 mol % F68 but lacking DMPG. $\Delta = 210$ ms (closed circles), 410 ms (open circles), 610 ms (closed triangles), and 810 ms (open triangles). For normal Gaussian diffusion, such decay curves for different diffusion times should overlap. (B) Normalized echo intensity decays versus $k^2\Delta^{1/2}$ for the same data as (A). For curvilinear, that is, non-Gaussian, diffusion, such decays for different diffusion times would overlap. The solid line was obtained using eq 7 with the fitting parameter $D^{1/2}\lambda = 1.02 \times 10^{-10} \text{ m}^2 \text{ s}^{-1/2}$.

the mean square displacements for different diffusion times, as obtained from the initial slopes of these decays as per eq 6, were plotted in a log–log fashion versus the diffusion time, a $\Delta^{1/2}$ -dependence became evident for diffusion times between 200 and 600 ms, as shown in Figure 10. There are a number of physical situations manifesting such as $\Delta^{1/2}$ -dependence, and these include reptation of polymer chains,⁴⁰ diffusion within or along giant wormlike micelles,⁴¹ and single-file diffusion.⁴² The common element is confinement of the diffusant to a one-dimensional curvilinear diffusion path. In such instances, the echo attenuation is given by

$$E(k, \Delta) = \exp(x^2) \text{erfc}(x) \quad (7)$$

(40) Fatkullin, N.; Kimmich, R. *Phys. Rev. E* **1995**, *52*, 3273–3276.

(41) Angelico, R.; Olsson, U.; Palazzo, G.; Ceglie, A. *Phys. Rev. Lett.* **1998**, *81*, 2823–2826.

(42) Kärger, J. *Phys. Rev. A* **1992**, *45*, 4173–4174.

(39) Vold, R. R.; Prosser, R. S. *J. Magn. Reson. B* **1996**, *113*, 267–271.

where

$$x = \frac{1}{3}(D\Delta)^{1/2}\lambda k^2 \quad (8)$$

in which λ is a characteristic distance identified with the persistence length of the curvilinear path. This dependence suggests that if the echo attenuation data are replotted as a function of $k^2\Delta^{1/2}$, decays obtained for different diffusion times should fall on a common master curve. As shown in Figure 11B, this indeed is found to be the case. The solid curve in Figure 11B was obtained with the fitting parameter $D^{1/2}\lambda = 1.02 \times 10^{-10} \text{ m}^2 \text{ s}^{-1/2}$. Note that when the echo attenuations for F68 in DMPG-containing bicellar mixtures are plotted in this same fashion, as shown in Figure 9B, no such common master curve is obtained, as expected given the normal Gaussian diffusion found in this situation.

The observation of curvilinear diffusion of F68 in neutral bicellar mixtures is consistent with the SANS results indicating ribbon structures. Assuming the intrinsic F68 diffusion coefficient to be the same in both neutral and charged bicellar mixtures, the fitted value of $D^{1/2}\lambda$ suggests a persistence length on the order of tens of micrometers. This conforms with the findings of van Dam et al.²⁵ who observed very long ($\gg \mu\text{m}$) quasi-cylindrical, highly branched structures in DMPC/DHPC bicellar mixtures using cryo-TEM.

When there is significant branching, or interconnectedness, of a network of one-dimensional diffusion paths, at long diffusion

times, the apparent diffusion eventually exhibits Gaussian behavior and recovers its diffusion time-independence. This crossover from non-Gaussian to Gaussian behavior occurs when the curvilinear displacement $\sim(2D\Delta)^{1/2}$ is greater than the curvilinear distance between branch points.⁴³ In Figure 11A, such a crossover appears to have taken place between $\Delta = 600$ and 800 ms, implying branch points separated by roughly 3–5 μm .

Conclusions

Through the combined use of SANS and NMR diffusion measurements, we have successfully characterized the structures of the magnetically alignable phase observed in DMPC/DHPC/F68 bicellar mixtures in the presence or absence of DMPG. Figure 4 summarizes the morphologies of DMPG-doped and non-DMPG-doped systems. In mixtures without DMPG, the lamellae are composed of meshed ribbons with an in-plane d -spacing of 120–140 Å and a persistence length of tens of μm . However, upon doping with 1 mol % of negatively charged DMPG, the in-plane morphology changes dramatically into a perforated lamellar structure, with no in-plane correlation. Moreover, the negative surface charge also allows the lamellae to swell. The mechanism that causes the in-plane structure to change upon addition of DMPG remains unclear. Pluronic F68 at the incorporation level studied here is not the cause of but rather, through its lateral diffusion, reports on these morphological differences.

Acknowledgment. Funded by the Natural Science and Engineering Research Council of Canada.

(43) Ambrosone, L.; Angelico, R.; Ceglie, A.; Olsson, U.; Palazzo, G. *Langmuir* **2001**, *17*, 6822–6830.